

MISR GLOBAL INFLIGHT GEOMETRIC CALIBRATION CONCEPT

Veljko M. JOVANOVIĆ and Michael M. SMYTH

*Jet Propulsion Laboratory, California Institute of Technology
4800 Oak Grove Drive, Mail Stop 169-315
Pasadena, CA 91109, USA*

ABSTRACT - The theoretical concept, underlying the design of the Multi-angle Imaging SpectroRadiometer (MISR) inflight geometric calibration is the subject of this paper. The algorithm is designed to provide data absolutely necessary for success of MISR autonomous georectification. Two main segments of calibration are related to the errors in the camera internal geometry and the errors in the supplied navigation and attitude data. The inflight calibration strategies rely on the use of global ground control points and digital elevation databases as well as on the unique instrument configuration of nine pushbroom cameras.

1 - INTRODUCTION

The MISR instrument is part of the payload for NASA's Terra spacecraft, which is scheduled to launch in November 1999. The purpose of MISR is to study the ecology and climate of the Earth through the acquisition of systematic, global multi-angle imagery in reflected sunlight. In order to derive geophysical parameters such as aerosol optical depth, bidirectional reflectance factor, and hemispheric reflectance, measured incident radiances from the multi-camera instrument must be coregistered. Furthermore, the coregistered image data and any subsequently derived product (e.g. cloud top heights) must be geolocated in order to meet experiment objectives such as: a) producing a data set of value to long-term monitoring programs and allowing intercomparisons of data on time scales exceeding that of an individual satellite, and b) providing Earth Observing System synergism by allowing data exchange between EOS-platform instruments.

In order to appropriately supply MISR scientific retrieval algorithms with data, the ground processing system has been built for continuous and autonomous coregistration and geolocation. The multiangle multispectral image data from nine fixed pushbroom cameras, housed by MISR instrument, are georectified to a common map projection. In response to the specific spatial accuracy requirements, we adopted a processing strategy which partitions effort between the MISR Science Computing Facility and the EOS Distributed Active Archive Center in a way that minimizes the amount of processing required at the latter location. Activities at the Science Computing Facility lower the computational need at the Distributed Active Archive Center by precalculating certain datasets early in the mission and staging them for on-going use, in a manner that eliminates excessive calculation during routine ground processing. The preparation of these ancillary datasets is done as a part of the global inflight geometric calibration utilizing a subset of MISR imagery and various datasets representing ground truth.

This paper describe the calibration algorithm and operational strategy focusing primarily on two issues: 1) possible errors in the internal camera geometric model and 2) possible errors in the supplied

ephemeris and attitude data. Section 2 gives an overview of the calibration approach. Section 3 present input dataset in more details, while Section 4 describe mathematical models and algorithm underlying the geometric calibration processing.

2 - OVERVIEW OF THE GEOMETRIC CALIBRATION

The in-flight geometric calibration operations are not part of standard processing. Instead, they will occur at the Science Computing Facility with the objective of producing a geometric calibration data set during the first six-eight months of the mission. This data set is used as an input to georectification processing in order to reduce processing load and provide the best possible input to automatic image registration. A comprehensive description of the MISR autonomous georectification, including the use of the geometric calibration data set is given in [9]. Production of a good quality geometric calibration dataset requires precise determination of the cameras interior geometry as well as determination of the instrument exterior orientation, taking into account errors in the supplied navigation and attitude. For that purpose, the following photogrammetric techniques will be used, such as: 1) space resection 2) simultaneous bundle adjustment and 3) combined feature/area based image matching.

The geometric calibration data set consist of two major parts: 1) Camera Geometric Model and 2) Projection Parameters and Reference Orbit Imagery.

The Camera Geometric Model data set is a set of parameters which are used in a mathematical expression that gives the pointing direction of an arbitrary pixel in reference to the spacecraft coordinate system (SCS). These parameters reflect geometries of the camera system and account for distortions (including temperature dependencies) from an ideal optical system [10]. Some of the parameters of the camera geometric model characterized during preflight ground calibration must be verified in orbit. It is expected that recalibrated camera geometric model will provide pointing vectors with accuracy of 1/8 of the pixel or better.

The full set of Reference Orbit Imagery (ROI) consists of selected cloud-free MISR imagery mosaicked and stored in the 233 files corresponding to the 233 orbit paths of the NASA's Terra spacecraft. Organized similarly into 233 files are the Projection Parameters (PP), which are produced off-line using rigorous photogrammetric reduction methods. The PP files provide geolocation information for acquired ROI's on a pixel by pixel basis. The major objective to be reached in order to produce pairs of the PP and ROI of required accuracy is the removal of errors in the supplied ephemeris and attitude data. In order to model these errors we used a simultaneous bundle adjustment utilizing multi-angle imagery.

The inflight geometric calibration processing starts with camera geometric model calibration via least-square space resection. Once the cameras are recalibrated the estimate of the ephemeris and attitude error models can begin. A pictorial description is given in Figure 1.

The camera calibration will use a set o globally distributed GCP's. The GCP's will be measured in corresponding MISR image segments acquired during a one month period. It is expected that during that period each GCP will be seen in at least three different orbit passes. The large number of observation is required in order to isolate static and systematic (e.g. temperature dependent) errors of the individual cameras from the errors in the navigation data.

The next calibration step is based on the simultaneous bundle adjustment which take advantage of MISR unique multiangle imaging capabilities. For that purpose the tie points measurement of the conjugate features across nine cameras are made. These measurements constrained with the already mentioned GCP's, a global digital elevation model, and a recalibrated camera internal geometries are used

to estimate errors of the ephemeris and attitude data for number of selected orbit passes. The plane is to perform this adjustment for about 30 percent of all MISR data that are acquired during a period of six months. This is optimal in regards to available SCF computing resources and will provide at least four orbit passes for the creation of reference orbit imagery corresponding to a single orbit path.

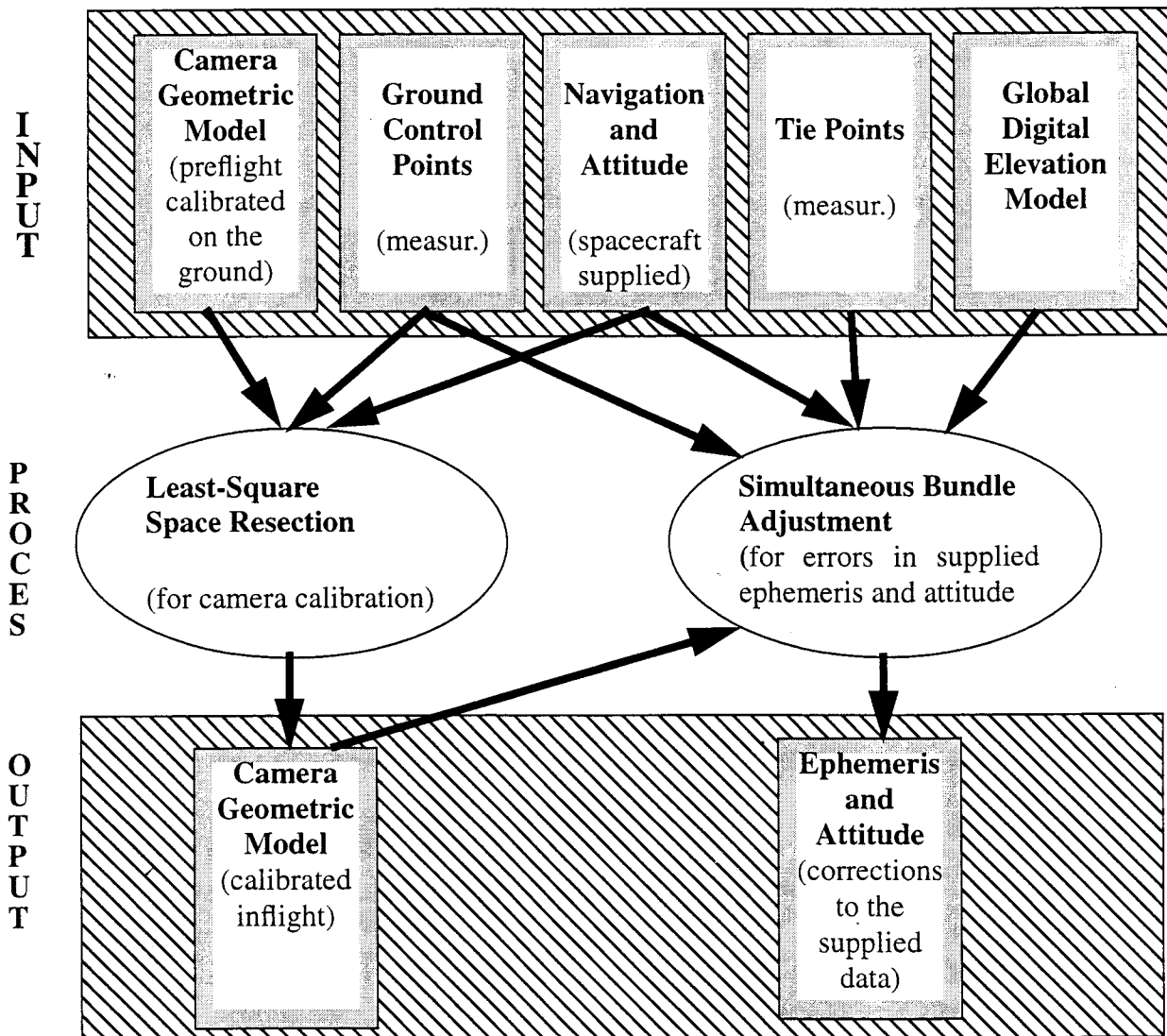


Fig. 1: Inflight geometric calibration process.

3 - INPUT DATA

3.1 - Camera Geometric Model

The MISR instrument consists of nine push-broom cameras. The cameras are arranged with one camera pointing toward the nadir (designated An), one bank of four cameras pointing in the forward direction (designated Af, Bf, Cf, and Df in order of increasing off-nadir angle), and one bank of four cameras pointing in the aftward direction (using the same convention but designated Aa, Ba, Ca, and Da). Images are acquired with nominal view angles, relative to the surface reference ellipsoid, of 0°, 26.1°, 45.6, 60.0°, and 70.5° for An, Af/Aa, Bf/Ba, Cf/Ca, and Df/Da, respectively. The instantaneous displacement in the along-track direction between the Df and Da views is about 2800 km (see Figure 2), and it takes about 7 minutes for a ground target to be observed by all nine cameras.

Each camera uses four charge-coupled device line arrays parallel in a single focal plane. The

line array contains 1504 photoactive pixels, each $21 \mu\text{m} \times 18 \mu\text{m}$. Each line array is filtered to provide one of four MISR spectral bands. The cross-track instantaneous field of view and sample spacing of each pixel is 275 m for all of the off-nadir cameras, and 250 m for the nadir camera. In order to simplify manufacturing, same optical design is used for nadir and Af/Aa off-nadir cameras, resulting in slightly different cross-track instantaneous fields of view. Along-track instantaneous fields of view depend on view angle, ranging from 250 m in the nadir to 707 m at the most oblique angle. Sample spacing in the along-track direction is 275 m in all cameras.

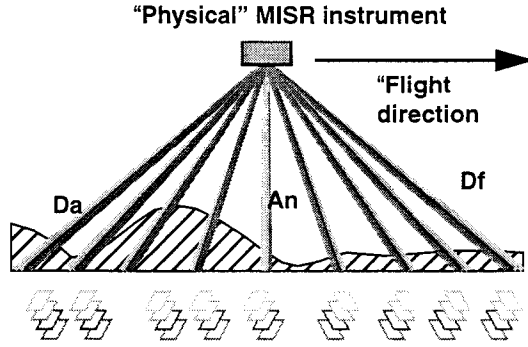


Fig. 2: MISR cameras configuration

In order to find the geolocation corresponding to a pixel's field of view, the pixel pointing direction is expressed in the geocentric coordinates system, as follows:

$$\hat{r}_{gci} = T_1 \hat{r}_{scs} \quad (1)$$

where \hat{r}_{scs} is the pixel pointing direction relative to the spacecraft coordinate system. T_1 , defined by the navigation and attitude data at the time of imaging, represents the transformation between the spacecraft and Geocentric coordinate system (see). The vector \hat{r}_{scs} is defined by the observable image coordinates and the set of constants which represent the instrument interior orientation parameters and transformation between the instrument and spacecraft coordinate axes. There will be nine sets of parameters corresponding to the nine MISR cameras.

These parameters are used to write a mathematical expression relating line and sample (l, s) coordinates of a band in one of the MISR cameras to the vector \hat{r}_{scs} in spacecraft coordinates system:

$$\hat{r}_{scs} = T_{si} \cdot T_{ic} \cdot T_{cd} \cdot \begin{bmatrix} -(k + (l - INT(l + 0.5))d_x) \\ f \sum_{i=0}^5 \alpha_i (s - c_y)^i \\ f \end{bmatrix} \quad (2)$$

where:

T_{si} is the rotation matrix function of the angles ($\omega_z, \omega_y, \omega_x$) between the spacecraft and instrument coordinate systems.

T_{ic} is the rotation matrix function of the angles ($\delta; \beta$) between the instrument and camera coordinate systems.

T_{cd} is the rotation matrix function of the angle ϵ between camera and detector coordinate systems.

k is the separation of the particular band from the intersection of the z axis with focal plane.

c_y is the pixel number (i.e., boresight pixel) corresponding to the x axis ($y = 0$).

d_x is the detector pitch in x direction.

f is the effective focal length.

α_i $i = 0, 1, 2, 3, 4, 5$ are the coefficients of a fifth-order polynomial to account for the nonlinear distortions of the field angle in the cross-track direction.

The camera geometric model has been calibrated on the ground prior to launch. A sample of the values obtained during preflight calibration is given in Table 1.

Table 1. Camera Geometric Model Parameters - a subset of preflight calibrated values for red band at 5°C. Sample for three cameras.

Cam.	Downtrack angle $k(3, 5)$ deg	f_0 (mm)	$\alpha(a_0, \dots)$	ϵ (deg.)	$\delta; \beta$ (deg.)	$\omega_z, \omega_y, \omega_x$ (deg.)
Df	-0.065	123.67	1.2747e-01	-0.2759	-28030 58.1266	0.006666 -0.041111 -0.0658333
An	-0.050	58.944	2.71992e-01	-0.1518	0.0022 0.0016	0.006666 -0.041111 -0.0658333
Da	-0.0358	123.653	1.2941e-01	0.0691	2.7314 -579879	0.006666 -0.041111 -0.0658333
Calibration						
Pre-flight	measured in lab at three temperatures	measured in lab at three temperatures	measured in lab at three temperature	measured in lab	measured in lab	measured once mounted on the S/C
In-flight	no	yes	yes	no	yes	yes
Sensitivity	none	thermal	thermal	none	thermal & gravity release	thermal and gravity release

A subset of these parameters will be affected by distortions resulting from the deformations of mechanical connections between the cameras, optical bench and the spacecraft platform, caused by launch and gravity release of the camera system. In that regards they (see Table 1) will be recalibrated inflight.

3.2 - Spacecraft ephemeris and attitude dataset

As pointed out earlier in equation (1), the spacecraft navigation and attitude data must be known to

relate a vector referenced to the spacecraft coordinate system (e.g., \hat{r}_{scs}) to the ground coordinate system,

The navigation data of interest to the in-flight geometric calibration are spacecraft position and velocity vectors. The navigation system uses a high accuracy output based on the TDRSS Onboard Navigation System (TONS) as the primary method of producing navigation data. The TONS navigation filter provides near real-time estimates of TERRA position and velocity every 10.24 seconds. The Guidance, Navigation and Control Subsystem (GN&CS), which provides position and velocity every 1.024 seconds, uses a second order Taylor series integrator to do estimation between TONS measurements. The position and velocity vectors are reported relative to the Geocentric Inertial Coordinate System of the mean Equator and Equinox of J2000. They are used to define the relation between the Orbital Coordinate System and the Geocentric Coordinate System at an instant of time. If \hat{P} is position and \hat{V} is velocity then the transformation between these two coordinate system can be written as:

$$T_{go} = \begin{bmatrix} \hat{x} & \hat{y} & \hat{z} \end{bmatrix} \quad (3)$$

where

$$\begin{aligned} \hat{z} &= \frac{\hat{P}}{\|\hat{P}\|} \\ \hat{y} &= \frac{\hat{z} \times \hat{V}}{\|\hat{z} \times \hat{V}\|} \\ \hat{x} &= \hat{y} \times \hat{z} \end{aligned} \quad (4)$$

The attitude data are produced through an attitude determination algorithm based on Kalman filtering theory. This algorithm receives measurements of stars or Sun and provides a 6-element state correction vector consisting of 3 small angle attitude errors and 3 gyro bias compensation errors. Calls are made to the Kalman update filter every 10 seconds, if stellar or solar measurements are available. At other times the attitude is propagated using gyros. The GN&CS provides attitude angles relative to the Orbital Coordinate System, and attitude rates relative to the Spacecraft Coordinate System every 1.024 seconds. The attitude angles, i.e., roll Ω , pitch Ψ , and yaw K , are used to define the transformation between the two coordinate systems:

$$T_{os} = \begin{bmatrix} \cos \Psi \cos K & \sin \Omega \sin \Psi \cos K - \cos \Omega \sin K & \cos \Omega \sin \Psi \cos K + \sin \Omega \cos K \\ \cos \Psi \sin K & \sin \Omega \sin \Psi \sin K + \cos \Omega \cos K & \cos \Omega \sin \Psi \sin K - \sin \Omega \cos K \\ -\sin \Psi & \sin \Omega \cos \Psi & \cos \Omega \cos \Psi \end{bmatrix} \quad (5)$$

Combining (5) and (3) with (2) the viewing direction expressed in the Geocentric Inertial Coordinate System is:

$$r_{gci} = T_{go} T_{os} r_{scs} \quad (6)$$

The TONS accuracy estimates and attitude determination accuracy estimates fall within the three-sigma navigation and attitude knowledge requirements. However, one of the goals of the inflight calibration is to remove unexpected and significant errors embodied in this data. For that purpose additional terms will be added to the model (6) and that topic is the subject of [1]. (4.2)

3.3 - Ground Control Points Measurements

Database

A single MISR ground control point is a collection of nine geolocated image patch of a well-defined and easily identifiable ground feature. The location of a particular ground feature is defined by corresponding geodetic coordinates. In our case, the ground feature is of type which can be found and precisely located in the applicable MISR image, using automated image matching. The optimal size (e.g., about 64x64 MISR pixels) of the image patch is driven by the image matching algorithm requirement. The accuracy of associated ground coordinates is expected to be 30 m for one sigma.

A completed MISR GCP's database will contain about 120 individual points distributed across all latitudes, the majority of which, about 60, are in the USA. About 50 points are equally distributed across Russian, African and South American regions. Remaining points are located in Australia / New Zealand region.

The construction of database involves two main processes. The first one is acquisition and production of terrain-corrected Landsat TM scenes over desired ground locations. The second one is extraction of image chips from the TM imagery and update of the GCP database. The selection of candidate ground location and TM scenes was done in collaboration with MODIS team and EROS Data Center. Seasonally invariant features (e.g., man-made objects, coastlines) are the first choice for GCPs. Once the Landsat TM scenes were selected EROS Data Center was responsible for precise geometric processing and terrain correction of these scenes prior to its distribution to the MODIS and MISR teams. This terrain corrected imagery is then used as the input to a ray casting simulation software. The software replicates MISR viewing geometry producing nine images (corresponding to nine MISR cameras) which are then used for the extraction of smaller image chips. This warping of TM imagery is necessary in order to obtain image chips with best possible chances to be identified in corresponding MISR imagery.

Purpose

Ground control points are used to detect errors in the pointing of a MISR camera for two purposes during in-flight calibration. First, and primarily, they are used to separate navigation errors from errors in the camera geometric model, enabling the update of the model parameters. Second, ground control points provide an excellent constraint while correcting for navigation and attitude data errors.

The centers of every GCP image chip are tagged with accurate geo-location. This ground location is expressed through the X_{ctr} , Y_{ctr} , and Z_{ctr} coordinates relative to the Conventional Terrestrial Reference Coordinate System (i.e., Earth fixed). Since the direction between the spacecraft center of mass (within ± 3 m) and the GCP is the same as the image viewing direction to that GCP, if both are expressed relative to the Geocentric System, the GCP is used to complement the collinearity model in the following way:

$$T_{gc} \begin{bmatrix} X_{ctr} \\ Y_{ctr} \\ Z_{ctr} \end{bmatrix} = \hat{P}_{gci} + k r_{gci} \quad (7)$$

where T_{gc} is the transformation between Conventional Terrestrial Reference and Geocentric Inertial coordinate systems at the instant of time when the GCP is observed. The coefficient k is a scale factor.

The \hat{P}_{gci} is the position of the spacecraft relative to the Geocentric Inertial coordinate systems. The r_{gci} is the viewing vector representing the function of the spacecraft attitude and the Camera Geometric Model. Equation (7) represent basic condition used during estimation of various parameters of the Camera Geometric Model.

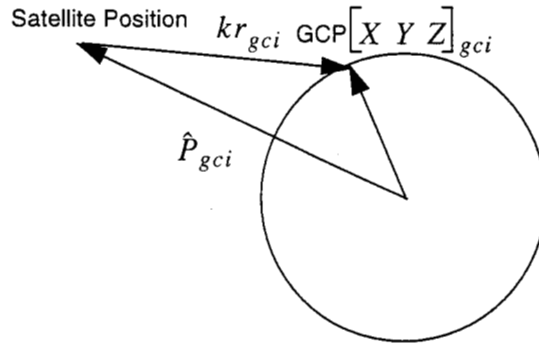


Fig. 3: GCP in relation to the camera vector

Identification

In order to be used during calibration GCP image chips must be precisely identified in applicable MISR imagery. The image location of the identified GCP must be measured and image line, and sample coordinate are passed as the input to the calibration program. The process of accessing, identifying and measuring GCP's is fully automatic. It is build on a combination of the area-based cross-correlation and least square image matching which shall provide measurements with accuracy of 1/8 of pixel for one sigma.

build

3.4 - Global Digital Elevation Model

Dataset

A seamless global Digital Elevation Map (DEM) is compiled from NIMA DTED-1 and other non-NIMA data sources. The dataset and special "retrieval" software are produced by the Cartographic Application Group (CAG) at JPL and are available to MISR for internal use. About 60% of DTED-1 are elevation posting provided on 100 m spacing with 30 m vertical accuracy which meet accuracy requirement of our calibration algorithm. Other portions of the dataset are of reduced accuracy but are still useful as the input to calibration.

The user of the dataset may specify size and location of the geographical grid with 3 arcsec spacing and obtain the following information on each of the 3 arcsec postings: 1) elevations in meters, relative to the Mean Sea Level, 2) flags indicating "land", "water", or "boundary" types of surface, and 3) meta-DEM data indicating source of the DEM postings and quality (accuracy) identifier.

During in-flight geometric calibration DID will be used to determine an equation of the surface over a small (max 6 x 6) rectangle. Such an equation of the surface is used as the constraint while modeling errors in the navigation and attitude data.

Initially, using only supplied navigation and attitude the ground location of the image point of interest will be determined. Then a rectangular grid of limited size of the elevation postings surrounding the ground point can be extracted from the DID. Using latitude, longitude (lat_i, lon_j , where $i, j = 0, 1, \dots, N$ is the size of the grid) and elevations (h_{ij}) a general function of the continuous interpolated surface of the form

$$h = P(lat, lon) \quad (8)$$

can be determined where P may belong to the family of either bilinear, biquadratic, or bicubic interpolating functions. During simultaneous bundle adjustment (Section 4.2) the least-square estimate of the ground coordinates ($X_{ctr}, Y_{ctr}, Z_{ctr}$), is made while removing errors from the navigation and attitude data. These ground coordinates will be additionally constrained with equation (8) when they are related to the lat, lon , and h as follows

$$\begin{aligned} X_{ctr} &= (N + h) \cos(lat) \cos(lon) \\ Y_{ctr} &= (N + h) \cos(lat) \sin(lon) \\ Z_{ctr} &= (N(1 - e^2) + h) \sin(lat) \end{aligned} \quad (9)$$

The equations (9) represent the transformation between Geodetic and Geocentric coordinate systems, where N is the ellipsoid radius of curvature in the prime vertical, and e is the ellipsoid eccentricity.

Without surface constraints (i.e., Equations (8) and (9)) modeling of the navigation and attitude errors will be limited to the relative effects only (utilizing multi-viewing capability of MISR). However, in order to account for absolute error, the surface equation is the second best constraint after the GCPs, which in some cases can be scattered too far from each other.

3.5 - Tie Points Measurements

While ground control points and global digital elevation inputs to calibration require preparation of datasets prior to launch the tie points measurements demand only availability of data obtained during flight. In particular, radiometrically corrected MISR Level 1 imagery and associated supplied spacecraft navigation and attitude are needed to obtain tie point measurements. The tie point is a ground feature which can be easily identified on multiple MISR imagery with the goal to accurately measure its image location on three or more camera views. The tie point measurements will produce a set of conjugate image locations which are then used as the ties between images obtained at different instant of time.

A thorough description of the tie points measurement algorithm is beyond the scope of this paper. In short, based on initial conjugate image locations determined using the knowledge of MISR navigation data, interest point features are detected independently on all 9 local conjugate image patches extracted from MISR imagery [5]. A feature-based matching scheme, namely consistent labeling with forward check [7], is then used to match conjugate interest points as improved tie-points, compared to the original ones. As the last step an area-based matching algorithm is then used to accurately identify the final tie-point with an uncertainty of less than 0.2 pixel. The tie-point identification is a completely automated process without human intervention. A supporting method with a human operator in the loop will be used mostly for validation purposes and for some infrequent occasions where improvement of the automatic detection of tie points is needed

4 - CALIBRATION ALGORITHM MATHEMATICAL DESCRIPTION

4.1 - Camera Calibration

The algorithm underlying mathematical model used for camera geometric calibration is based on least-square space resection method exploited in frame photogrammetry.

Looking back on Figure 3, the statement can be made that the camera, GCP and image of that point all must be aligned. The mathematical term expressing this geometric condition is the collinearity condition. The final form, which is going to be used in this calibration, can be derived from the equation (7). Let us propose that $G_{gci} = T_{gc} \times [X_{ctr} \ Y_{ctr} \ Z_{ctr}]^T$ is the GCP vector in the Geocentric Inertial frame. Then (7) can be rearranged as:

$$k \cdot r_{gci} = G_{gci} - P_{gci} \quad (10)$$

The vector r_{gci} is derived (subsections §3.1 and §3.2), to be:

$$r_{gci} = \mu \cdot T_{go} T_{os} T_{si} T_{ic} T_{cd} r_{dcs} \quad (11)$$

In order to further rearrange (10), the transformation from the Geocentric Inertial to the Detector coordinate system is set to be $M = [T_{go} T_{os} T_{si} T_{ic} T_{cd}]^T$, so that

$$r_{dcs} = \frac{1}{k\mu} \cdot M \times [G_{gci} - P_{gci}] \quad (12)$$

or further (dropping out the subscripts which denote coordinate system)

$$\begin{bmatrix} -x_f \\ -y_f \\ f \end{bmatrix} = \frac{1}{k\mu} \cdot \begin{bmatrix} m_{11} & m_{12} & m_{13} \\ m_{21} & m_{22} & m_{23} \\ m_{31} & m_{32} & m_{33} \end{bmatrix} \times \left[\begin{bmatrix} G_x \\ G_y \\ G_z \end{bmatrix} - \begin{bmatrix} P_x \\ P_y \\ P_z \end{bmatrix} \right] \quad (13)$$

Expanding the right hand side and dividing the first two equation by the third, leads to collinearity condition equations:

$$\begin{aligned} F_1(obs, par) &= x_f + f \cdot \frac{m_{11} \cdot (G_x - P_x) + m_{12} \cdot (G_y - P_y) + m_{13} \cdot (G_z - P_z)}{m_{31} \cdot (G_x - P_x) + m_{32} \cdot (G_y - P_y) + m_{33} \cdot (G_z - P_z)} = 0 \\ F_2(obs, par) &= y_f + f \cdot \frac{m_{21} \cdot (G_x - P_x) + m_{22} \cdot (G_y - P_y) + m_{23} \cdot (G_z - P_z)}{m_{31} \cdot (G_x - P_x) + m_{32} \cdot (G_y - P_y) + m_{33} \cdot (G_z - P_z)} = 0 \end{aligned} \quad (14)$$

which will be used as the mathematical model in the least-square resection. Since the equations (14) are non-linear the linearized form for a single ray (j th GCP seen on i th MISR image) would be:

$$a_{j,i} v_{j,i} + b_{j,i} \Delta = f_{j,i}^0 \quad (15)$$

where:

Table 3: Sensitivity to Attitude Errors (camera pixel 0, red band)

Camera	Yaw + 10 arcseconds		Pitch + 10 arcseconds		Roll + 10 arcseconds	
	Along track (meter)	Cross track (meter)	Along track (meter)	Cross track (meter)	Along track (meter)	Cross track (meter)
BF	-12	-30	67	-7	-11	39
AF	-11	-15	42	-3	-5	38
AN	-9	-1	34	3	0	41
AA	-10	15	42	8	4	38
BA	-10	30	70	14	8	39
CA	-10	47	122	22	12	41
DA	-11	67	247	35	17	44

As can be seen, we are not equally sensitive to each of the attitude angles. We are far more sensitive to pitch than any of the other angles. The effect of yaw and roll are roughly the same, and are largely in the cross track direction.

Attitude Error Model

The error term E_{attitude} is a slowly varying function. We intend on modeling it by a spline curve. The spline is a piecewise cubic polynomial, with coefficients selected so that the value of polynomial and its derivative at the location of the knots match the given position and velocity of the knot. For the polynomial valid between knot i and $i + 1$ with angle at t_i of a_i , rate at t_i of a'_i and an angle and rate at time t_{i+1} of a_{i+1} and a'_{i+1} we have:

$$a = c_0^i + c_1^i \frac{t-t_i}{t_{i+1}-t_i} + c_2^i \left(\frac{t-t_i}{t_{i+1}-t_i} \right)^2 + c_3^i \left(\frac{t-t_i}{t_{i+1}-t_i} \right)^3 \quad (55)$$

$$c_0^i = a_i \quad (56)$$

$$c_1^i = a'_i (t_{i+1} - t_i) \quad (57)$$

$$c_2^i = 3(a_{i+1} - a_i) - (a'_{i+1} + 2a'_i)(t_{i+1} - t_i) \quad (58)$$

$$c_3^i = -2(a_{i+1} - a_i) + (a'_{i+1} + a'_i)(t_{i+1} - t_i) \quad (59)$$

The location of knots in the spline are determined so that the resulting spline models the attitude error closely enough to meet the error budget for the simultaneous bundle adjustment. As shown

a is a 2x2 matrix of partial derivatives with respect to observations.

v is a 2x1 vector of observational residuals.

b is a 2x3 matrix of partial derivatives with respect to CGM parameters β , δ and ϵ which are going to be calibrated.

Δ is a 3x1 vector of parameter corrections

f^0 is a pair of functions evaluated at the actual observations and initial values (pre-flight CGM) of the parameters of interest.

Now, let's say that the q is 2x2 variance-covariance matrix of the line and sample observations for a GCP. Given n GCPs seen in m MISR images a solution of the $(n \times m)$ system of the equations of type (15) can be written as:

$$\Delta = N^{-1}T \quad (16)$$

where 3x3 matrix N^{-1} can be evaluated as

$$N^{-1} = \left(\sum_{j=1}^n \sum_{i=1}^m b_{j,i}^T (a_{j,i} q_{j,i} a_{j,i}^T)^{-1} b_{j,i} \right)^{-1} \quad (17)$$

and 3x1 matrix T as

$$T = \left(\sum_{j=1}^n \sum_{i=1}^m b_{j,i}^T (a_{j,i} q_{j,i} a_{j,i}^T)^{-1} f_{j,i}^0 \right) \quad (18)$$

The least-square solution is iterative, and since the initial values of the parameters would be close to their real value (results of pre-flight calibration), the convergence would be of second order and relatively fast. The criteria for termination of iterations is based on the fact that parameter correction should approach zero.

4.2 - Simultaneous Bundle Adjustment

The navigation and attitude data may contain errors which could, when propagated, reduce the accuracy of the geo-location and co-registration to an unacceptable level. The goal of this calibration is to model and estimate time-dependent error functions. When used with the already supplied navigation and attitude data and inflight calibrated camera geometric model during these error functions will assure pointing with acceptable accuracy.

The basic ideas characterizing this approach are as follows:

- a) Takes advantage of MISR multi-viewing capability: at an instant of time the MISR instrument observes (simultaneously) nine different locations on the ground. Consequently, a single ground point is seen at nine different instants of time. Through the use of tie points a strong connection between discrete navigation and attitude data can be made, so that estimation of a time dependent error function is feasible.
- b) Models the attitude and ephemeris knowledge errors according to a physical model of the measurement devices.
- c) Uses a global digital elevation model as a constraint for the adjustment.
- d) Uses available ground control points as a constraint for the adjustment.

- e) Uses a nonlinear least squares technique to determine the best fit of the parameters of attitude and ephemeris error model.
- f) During initial testing of the system, evaluates how well our orbit measurement model models the real Terra orbit.

Ephemeris Measurement/Error Model

The TDRSS Onboard Navigation System (TONS) is used to produce estimates of the Terra ephemeris at 10.24 second intervals, during those times that contact with the TDRSS can be established. Contact with the TDRSS satellite can not be maintained throughout the whole Terra orbit. There are two contacts per orbit, each lasting for about 10 minutes. In between estimates from TONS, a real-time interface algorithm is used to propagate the ephemeris.

The largest ephemeris errors occur during the times between TDRSS contacts. The most important error term in the real-time interface algorithm is a drag term that is not fully accounted for. This error term leads to errors mostly in the along track direction, and is close to linear in time.

This gives the following measurement model:

$$X^{measured} = X^{true} + a(t - t_0) + b \quad (19)$$

The measurement model for $Y^{measured}$ and $Z^{measured}$ are identical. It should be pointed out that this is done in the orbital coordinate system, so that $Z^{measured}$ is in the radial direction, $X^{measured}$ is in the along track direction, and $Y^{measured}$ is in the cross track direction.

Attitude Measurement Model

The attitude of the “Terra” spacecraft is measured by a combination of two instruments, a pair of solid state star trackers (SSST) and an inertial reference unit (IRU), made up of three gyros and an associated computer. A fine sun sensor (FSS) is used as a backup if one of the SSSTs fails.

The attitude is determined by a Kalman filter. The filter is updated every 10 seconds, if SSST or FSS sensor measurements are available. The filter updates a six-element state vector consisting of three small angle attitude errors and three gyro bias compensation errors. At other times, the attitude is propagated using the IRU.

The two SSSTs will generally see a star every 10 seconds. However, given certain circumstances, a substantial interference by the moon can occur, preventing a filter update for as long as 20 minutes. If the FSS is being used because one of the SSSTs fails, measurements of the sun will be made every 10 seconds while the sun is visible. However, the FSS can only be used for about 22 minutes out of the 90 minute orbit.

Between the SSST/FSS measurements, the IRU is used to determine the attitude rates. The IRU consists of three rate-integrating gyros operating in a torque rebalance strap-down mode. The gyro rates are measured every 0.128 seconds, and the attitude and rates are updated every 0.512 seconds.

The star tracker measurement is modeled as:

$$A_{measured} = A_{true} + E_{static} + E_{dynamic} \quad (20)$$

Where A refers to one of the attitude angles; roll, pitch, or yaw.

The IRU measurement is modeled as:

$$\Delta A_{\text{measured}} = \Delta A_{\text{true}} + E_{\text{bias}} + E_{\text{gyro white noise}} \quad (21)$$

We can combine the two measurement models to give:

$$A_{\text{measured}} = A_{\text{true}} + E_{\text{attitude}} \quad (22)$$

Where E_{attitude} is slowly varying, changing on the scale of tens or hundreds of seconds. We intend on modeling it by a spline curve. The spline is a piecewise cubic polynomial, with coefficients selected so that the value of polynomial and its derivative at the location of the knots match the given position and velocity of the knot. For the polynomial valid between knot i and $i + 1$ with angle at t_i of a_i , rate at t_i of a'_i and an angle and rate at time t_{i+1} of a_{i+1} and a'_{i+1} we have:

$$a = c_0^i + c_1^i \frac{t - t_i}{t_{i+1} - t_i} + c_2^i \left(\frac{t - t_i}{t_{i+1} - t_i} \right)^2 + c_3^i \left(\frac{t - t_i}{t_{i+1} - t_i} \right)^3 \quad (23)$$

$$c_0^i = a_i \quad (24)$$

$$c_1^i = a'_i (t_{i+1} - t_i) \quad (25)$$

$$c_2^i = 3(a_{i+1} - a_i) - (a'_{i+1} + 2a'_i)(t_{i+1} - t_i) \quad (26)$$

$$c_3^i = -2(a_{i+1} - a_i) + (a'_{i+1} + a'_i)(t_{i+1} - t_i) \quad (27)$$

The location of knots in the spline are determined so that the resulting spline models the attitude error closely enough to meet the error budget for the simultaneous bundle adjustment. It has been shown that our sensitivity to pitch errors is much larger than to yaw and roll errors. This suggests that we actually want to use a different spacing of knots for each of the attitude angles; we can tolerate fewer knots for the yaw and roll.

We intend on using equal spaced knots, with the spacing adjusted to give acceptable accuracy of the attitude. However, a specific knot might not have enough tie points or sufficient camera coverage around it to determine the knot parameters. We remove knot i if:

$$\sum_{\text{cameras}} N_{\text{tie point seen}}(t_i, t_{i+1}, \text{camera}) < \text{Threshold1} \quad (28)$$

or

$$\sum_{\text{camera}} \{1 \text{ if } (N_{\text{tie point seen}}(t_i, t_{i+1}, \text{camera}) \neq 0), 0 \text{ otherwise}\} < \text{Threshold2} \quad (29)$$

Collinearity Constraint

The collinearity condition equations (14) derived in the previous section, in a general sense, are also applied for the model of simultaneous bundle adjustment. In this case, the ground coordinates of a tie point are not actually known (only approximately) but are common in association with multiple pairs

of image coordinates of the same tie point seen in multiple camera views. If we use i as the index for tie points and j as the camera index, then a form of (14) can be written as a system of equations:

$$\begin{aligned} F_1^{ij}(l^{ij}, P_i, EphemerisModel, AttitudeModel, \dots) &= 0 \\ F_2^{ij}(s^{ij}, P_i, EphemerisModel, AttitudeModel, \dots) &= 0 \end{aligned} \quad (30)$$

where l^{ij} and s^{ij} are image coordinates of i -th tie point in j -th cameras. The tie point ground location P_i along with the ephemeris and attitude error models are to be computed via this estimation. Only initial values and corresponding a priori covariance matrix are given as the input. In the words system of equations (30) is based on the constraint that the image location of a tie point predicted by ephemeris and attitude model match the actual image location obtained through the tie point matching. In general, this system of equations cannot be solved exactly, so the equality should be taken in a least squares sense, weighted by the appropriate covariance matrixes.

Surface Constraint

While estimating the location of P_i , we want to take advantage of the fact that we have a description of the surface pertained in a global digital elevation model. Since we know a tie point is going to lie on a surface, we add the following to our series of equations:

$$h(\text{lattitude}(P_i), \text{longitude}(P_i)) - H(P_i) = 0 \quad (31)$$

where height h is obtained using a global digital elevation model and a surface interpolation function, while height H is obtained by a transformation between Geocentric and Geodetic coordinates systems defined in (9).

Again, this set of equations are to be taken in the least squares sense, weighted by the uncertainty of the particular value in the digital elevation model.

Ground Control Point (GCP) Constraint

We have collected a set of GCPs for camera calibration, which we want to take advantage of during the simultaneous bundle adjustment. We treat the GCPs as any other tie point, using a system of equations like (30) to impose the collinearity constraint. In addition, we want to constrain the location of P_i to the known location of the ground control point P_i^{GCP} . We do this by adding the following to our series of equations:

$$P_i^{GCP} - P_i = 0 \quad (32)$$

Again, this equation is to be taken in the least squares sense, weighted by the covariance matrix of the GCP location.

Solution of System of SBA Equations

We adopted to solve the nonlinear system of equations (30), (31), and (32) by doing numerical linearization and using the standard Levenberg-Marquardt method (see [4]).

The Levenberg-Marquardt method is used to minimize $F^T(x)WF(x)$. In our particular example, F represented evaluated system of equations. W is the weight matrix, which is the inverse of the apriori

covariance matrix. The algorithm is iterative, calculating new value of x by:

$$x_n = x_{n-1} - (J^T(x_{n-1})WJ(x_{n-1}) + \lambda I)^{-1}J^T(x_{n-1})WF(x_{n-1}) \quad (33)$$

where J is the Jacobian and λ is a parameter controlling how large of a step we make take in the steepest descent direction. The algorithm iterates until a stopping criteria is reached, such as having the residuals $F(x_n)$ being sufficiently small.

The covariance of the resulting parameters is given by

$$C = (J^T(x_{n-1})WJ(x_{n-1}) + \lambda I)^{-1} \quad (34)$$

5 - CONCLUSION

MISR autonomous georectification data reduction is a unique process requiring specialized type of the inflight geometric calibration operations. The algorithms providing theoretical basis for these operation have been implemented and tested using simulated data. Our test cases and simulated data have been based on the wide range of possible conditions in terms of specified and required accuracies as well as the distribution of ground control and tie points. In addition to the operational code we have developed a number of tools to help as during initial algorithm / software validation efforts. Availability of real image data is required in order to fully tuned up algorithm focusing on the elements such us: a) exact set of the camera parameters to be calibrated, b) possible correlation between parameters across different cameras, c) validity of the ground control points database - eliminate possible blunders, d) determine optimal ephemeris error model, e) determine optimal attitude error model including the number of knots and threshold used for knots elimination.

6 - ACKNOWLEDGMENT

The authors gratefully acknowledge the efforts of the MISR Principal Investigator, David J. Diner, the Science Data Production System manager Graham Bothwell, and the members of the Science Data System Team: Earl G. Hansen, Mike Bull, and Jia Zong. Additional thanks are due to Carol J. Bruegge and Robert P. Korechoff for their efforts in MISR preflight camera calibration. This work is being carried out at the Jet Propulsion Laboratory, California Institute of Technology, under contract with the National Aeronautics and Space Administration.

References

- [1] Ackermann, F., "Digital Image Correlation: Performance and Potential Application in Photogrammetry", *Photogrammetric Record*, **11**, 64, 1984.
- [2] Allison, D., Barnsley, M. J., Lewis P., Dyble N., and Muller, J.P., "Precise Geometric Registration of ASAS Airborne Data for Land Surface BRDF Studies", *IGARSS Proceedings*, **3**, 1655-1657, 1994.
- [3] Dennis, J. E. Jr. and Schnabel, Robert B., Numerical Methods for Unconstrained Optimization and Nonlinear Equations, Prentice-Hall, NJ., 1983.
- [4] Diner, D. J., Beckert, J. C., Reilly, T. H., Bruegge, C. J., Conel J. E., Kahn, R. A., Martonchick, J. V., Ackerman T. P., Davis, R., Gerstl, S. A. W., Gordon, H. R., Muller, J. P., Myneni, R., Sellers, P. J., Pinty, B., and Verstraete, M. M., "Multi-angle Imaging SpectroRadiometer (MISR) Instrument Description and Experiment Overview", *IEEE Trans. Geosci. Remote Sens.*,
- [5] Forstner, W., "A Fast Operator for Detection and Precise Location of Distinct Points, Corners and Centers of Circular Features", *ISPRS Intercommission Workshop, InterLaken*, 1987.
- [6] Forstner, W., "On the Geometric Precision of Digital Correlation", *ISPRS Int. Arch. of Photogrammetry*, vol. XXIV, Commission III, Helsinki, 1980.
- [7] Haralick, R., Shapiro, L., "Computer and Robot Vision", Addison-Wesley Publish Company, 1993.
- [8] Herrick, S., "Astrodynamics", Van Nostrand Reinhold, New York, 1971.
- [9] Jovanovic, V. M., Smyth, M. M., Zong, J., Ando, R., and Bothwell, G., W., "MISR Photogrammetric Data Reduction for Geophysical Retrievals", *IEEE Transaction on Geoscience and Remote Sensing*, Vol. 36, No. 4, July 1998.
- [10] Korechoff, R. P., Jovanovic, V. M., Hochberg, E. B., Kirby, D. M., and Sepulveda, C. A., "Distortion calibration of the MISR linear detector arrays", *SPIE Proceedings* Volume 2820-19, Denver, Colorado August 1996.
- [11] Lewicki, S. A., Smyth, M. M., Jovanovic, V. M., and Hansen, E. G., "A Simulation of EOS MISR Data and Geometric Processing for the Prototyping of the MISR Ground Data System", *IGARSS Proceedings*, **3**, 1543-1545, 1994.
- [12] Mikhail, E. M., "Observations and Least Square", Harper & Row, New York, 1976.
- [13] Muller, J. p., Mandanayake, A., Davis, R., and Moroney, C., "A comparison of stereo matching techniques for Global Cloud-top Height retrieval from ATSR and MISR", *J. Geophys. Res.*, in preparation, 1997.
- [14] Paderes, F. C., Mikhail, E. M., and Fagerman, J. A., "Batch and On-Line Evaluation of Stereo Spot Imagery", *ASPRS Proceedings*, **3**, 1989.

[15] Snyder, J. P., "Map Projection - A Working Manual", United States Geological Survey Professional Paper 1395, U. S. Government Printing Office, Washington, 1987.

[16] Zong, J., Jovanovic, V. M., and Smyth, M. M., "MISR band-to-band registration", *SPIE Proceedings* Volume 2818-28, Denver, Colorado August 1996.